

## Thermally driven state in a spin-1 model with competing interactions

G. L. K. Frantz and M. Schmidt *Departamento de Física, Universidade Federal de Santa Maria, 97105-900 Santa Maria, RS, Brazil*F. M. Zimmer *Instituto de Física, Universidade Federal de Mato Grosso do Sul, 79070-900 Campo Grande, MS, Brazil* (Received 19 November 2020; revised 1 February 2021; accepted 17 February 2021; published 17 March 2021)

We study a recently proposed spin-1 model with competing antiferromagnetic first-neighbor interaction and a third-neighbor coupling mediated by nonmagnetic states, which reproduces topological features of the phase diagrams of high- $T_c$  superconductors [S. A. Cannas and D. A. Stariolo, *Phys. Rev. E* **99**, 042137 (2019)]. We employ a cluster mean-field approach to investigate effects of crystal field anisotropy on the phase transitions hosted by this model. At low temperatures, the temperature-crystal field phase diagram exhibits superantiferromagnetic (SAF), antiferromagnetic (AF), and paramagnetic (PM) phases. In addition, we found a thermally driven state between SAF and PM phases. This thermally driven state and the SAF phase appears in the phase diagram as a domelike structure. Our calculations indicate that only second-order phase transitions occur in the PM-AF phase boundary, as suggested by previous Monte Carlo simulations.

DOI: [10.1103/PhysRevE.103.032125](https://doi.org/10.1103/PhysRevE.103.032125)

### I. INTRODUCTION

Competing interactions in strongly correlated materials are a continuous source of complex and novel phenomena. Despite decades of active research, describing many of these systems still remains a challenge for both theoretical and experimental standpoints. In particular, relevant insights into the physics of correlated systems have been revealed by the study of interacting spin models. Although incorporating a reduced number of degrees of freedom, magnetic models have allowed us to unveil mechanisms underlying several interesting phenomena, such as order by disorder [1–3], inverse transitions [4–6], and quantum criticality [7–9], to name a few. Central to the advances achieved so far is the proposal of models capable to incorporate the basic features of more complex systems. Recently, a three-state pseudospin model with competing antiferromagnetic and pairing interactions has been proposed by Cannas and Stariolo (CS) [10] to reproduce the structure found in phase diagrams of high-temperature superconductors [11,12], including antiferromagnetic long-range order and a domelike phase boundary. However, several aspects of this model, such as the nature of phase transitions and possible other types of orderings, still deserve further attention. In the present work, we investigate the phase diagram of the CS model by means of cluster mean-field (CMF) calculations.

The three-state CS model [10] considers two types of interactions: an antiferromagnetic (AF) interaction ( $J_A$ ) between first-neighbors and a third-neighbor AF coupling  $J_B$ , which is mediated by holes (represented by nonmagnetic spin states). The latter can be seen as a type of three-site four spin

interaction, which can drive a rather unusual form of long-range order, the so called superantiferromagnetic (SAF) phase. In this state, the system is divided into two interpenetrated sublattices: one with very low local magnetization and the other showing an AF pattern (see Fig. 1). For a relevant strength of the interactions ( $J_B = 2J_A$ ), effects of chemical potential ( $\mu$ ) on the competition between ordered phases were evaluated within standard mean-field approach and Monte Carlo simulations [10]. At low temperature ( $T$ ), tuning the chemical potential can lead to the onset of a SAF state, which appears in a domelike structure in the  $T$ - $\mu$  plane. In addition, the ground state changes from the SAF phase to an AF phase when magnetic states are favored by  $\mu$ . Therefore, the CS model is able to reproduce the topology of the phase diagrams of high-temperature superconductors induced by hole doping.

Despite the ground-state transitions are established for the CS model, the mean-field calculation and Monte Carlo simulations lead to rather different descriptions for the nature of the phase transitions in the CS model [10]. One of the relevant discrepancies concerns the transition line between paramagnetic (PM) and SAF phases: while Monte Carlo results indicate the presence of both first- and second-order phase transitions, standard mean-field findings suggest only first-order phase transitions. Moreover, for the PM-AF phase boundary, mean-field calculations indicate the presence of both first-order and second-order phase transitions, but no evidence of first-order phase transitions are found within Monte Carlo results. Therefore, further studies of the CS model are required to shed some light on the nature of phase transitions. It also should be noted that additional investigations can unveil novel and unexplored features of the model.

The description of phase transitions in models with competing interactions often represent a challenge for theorists. While the simplest approach—the standard single-site

\*mschmidt@mail.ufsm.br

†fabiozimmer@gmail.com

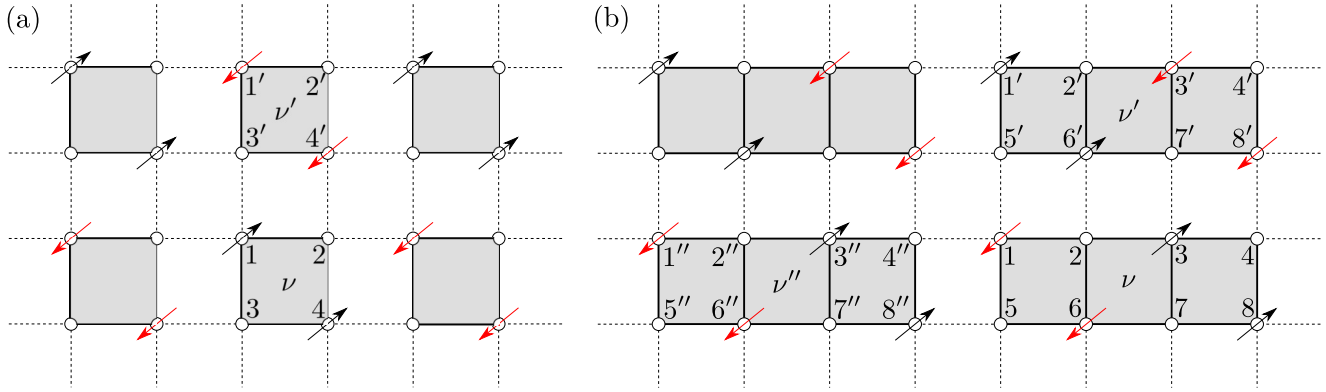


FIG. 1. Representation of the clusters considered in the CMF approach with (a)  $n_s = 4$  and (b)  $n_s = 8$ . In the reference system, the clusters are decoupled from the neighborhood and only intercluster interactions (solid lines) are treated exactly. The intercluster interactions (dashed lines) are evaluated within a mean-field procedure. The SAF ground-state is depicted with arrows representing the magnetic states ( $S_i = \pm 1$ ) and empty circles denoting the nonmagnetic states ( $S_i = 0$ ).

mean-field theory—allows a straightforward description of phase boundaries, this method neglects effects of correlations, which can be relevant for the nature of phase transitions [13]. However, Monte Carlo simulations allows to incorporate the role of correlations, but classifying phase transitions can be very tricky within this approach, in which finite-size effects should be taken into account [14,15]. Therefore, alternatives to these methods are often required to describe phase boundaries. A method that allows to incorporate short-range correlations and still provides a simple framework to evaluate the nature of phase transitions is the cluster mean-field theory. The method consists in evaluating exactly the interactions within a given cluster, while the intercluster couplings are computed in a mean-field fashion [16–18]. The CMF theory has been recently employed in the study of several systems with competing interactions [18–29], often providing an accurate description for the nature of phase boundaries [18,27–29]. Motivated by the issues concerning the nature of phase transitions of the CS model, we propose a CMF investigation of this model, with particular focus on the nature of phase transitions and the possible onset of other ordered states.

The paper follows with the model definition and its treatment within the cluster mean-field theory in Sec. II. In Sec. III, we present a detailed discussion of the obtained results. We present our conclusion in Sec. IV.

## II. MODEL

We considered the spin-1 model proposed by Cannas and Stariolo [10], which is given by the Hamiltonian

$$H = -J_A \sum_{\langle i,j \rangle} S_i S_j - J_B \sum_{\langle\langle i,j,k \rangle\rangle} (1 - S_i^2) S_j S_k - D \sum_i S_i^2, \quad (1)$$

where  $S_i$  represents the spin variables placed at the vertices of a square lattice, which can assume three different states  $S_i = \pm 1, 0$ . The first sum, denoted by  $\langle i, j \rangle$ , runs over first-neighbors and incorporates an interaction of strength  $J_A$ . The second term accounts for a third-neighbor coupling of strength  $J_B$ , which is mediated by nonmagnetic states ( $S_i = 0$ ). It is also worth to mention that this coupling is expected to mimic a pairing interaction [10]. The sum denoted by  $\langle\langle i, j, k \rangle\rangle$  runs

over sites  $i, j$  and  $k$ , such that  $j$  is a third neighbor of  $k$  and  $i$  is a first neighbor of both  $j$  and  $k$ . The last term in the Hamiltonian incorporates the crystal field  $D$ , which can be used to tune the energetic favoring of magnetic (when  $D > 0$ ) or nonmagnetic states (when  $D < 0$ ). In this way, the crystal field plays an analogous role of the chemical potential considered by the authors of the model [10]. Following Ref. [10], we considered both couplings to be antiferromagnetic ( $J_A = -1$  and  $J_B = -2$ ). We note that a negative  $J_A$  favors a parallel alignment between third neighbors, acting against the antiferromagnetic coupling between third neighbors  $J_B$ . Thus, there is a competition between  $J_A$  and  $J_B$ .

To investigate the model of Eq. (1), we considered a CMF approximation [18], based on the Bogoliubov inequality

$$F \leq \phi = F_0 + \langle H - H_0 \rangle_0, \quad (2)$$

where  $F$  is the free energy of the original system,  $F_0$  is the free-energy of a reference system with Hamiltonian  $H_0$ , and  $\langle \dots \rangle_0$  denotes an average with respect to  $H_0$ . In this work, we considered that the reference system is composed of  $N_{cl}$  clusters with  $n_s$  sites each. The spins on this clusters are coupled with intracluster neighbors (for  $n_s > 1$ ) and with variational parameters, which means that the clusters are decoupled from the neighborhood. We note that the cluster size and shape considered are relevant to the outputs of this method. In the present work, we considered four levels of approximation: the single-site approximation and clusters with  $n_s = 4$  [Fig. 1(a)],  $n_s = 8$  [Fig. 1(b)], and  $n_s = 12$  (Fig. 11). In the following, we discuss the CMF procedure for  $n_s = 4$ , providing details for  $n_s = 1, 8$ , and 12 in the Appendices A, B, and C, respectively.

For  $n_s = 4$ , our reference system is a square lattice divided in identical square clusters, as illustrated in Fig. 1(a). Then,  $H_0$  can be written as a sum of the Hamiltonians of each cluster, so we can express it as  $H_0 = \sum_v^{N_{cl}} H_0^v$ . The Hamiltonian of a single cluster  $v$  is given by

$$H_0^v = H_{in} - \sum_{i \in v} \eta_i S_i - \sum_{(i,k \in v)} \lambda_{i,k} S_i^2 S_k, \quad (3)$$

where

$$H_{\text{in}} = -J_A \sum_{(i,j \in \nu)} S_i S_j - D \sum_{i \in \nu} S_i^2, \quad (4)$$

with the first sum running over the intracluster first neighbors, with each pair counted only once. The variational parameters  $\eta_i$  and  $\lambda_{i,k}$  are coupled to single sites ( $S_i$ ) and pairs of sites ( $S_i^2 S_k$ ), respectively. In addition,  $(i, k \in \nu)$  indicates a sum over all sites ( $i$ ) of the cluster  $\nu$  and its intracluster nearest neighbors ( $k$ ).

To evaluate the last term in Eq. (2) we divided the original system into  $N_{\text{cl}}$  interacting clusters. In this way, we can write

$$\begin{aligned} \langle H^\nu \rangle_0 = & -J_A \sum_{(i,j \in \nu)} \langle S_i S_j \rangle_0 - \frac{J_A}{2} \sum_{(i,j')} \langle S_i S_{j'} \rangle_0 \\ & - J_B \sum_{\langle(i,j',k) \rangle} \langle (1 - S_i^2) S_{j'} S_k \rangle_0 - D \sum_{i \in \nu} \langle S_i^2 \rangle_0, \end{aligned} \quad (5)$$

where  $(i, j')$  in the second sum refers to intercluster interactions where  $i$  belongs to cluster  $\nu$  and  $j'$  belongs to a cluster in the neighborhood of  $\nu$ . The  $1/2$  factor is adopted to avoid double counting of the interactions. The third sum accounts for the intercluster couplings mediated by nonmagnetic states, where  $i$  and  $k$  belongs to  $\nu$  and  $j'$  belongs to a neighbor cluster.

As the averages are taken with respect to a system of decoupled clusters, we can write

$$\langle S_i S_{j'} \rangle_0 = \langle S_i \rangle_0 \langle S_{j'} \rangle_0, \quad (6)$$

and

$$\langle (1 - S_i^2) S_{j'} S_k \rangle_0 = \langle (1 - S_i^2) S_k \rangle_0 \langle S_{j'} \rangle_0. \quad (7)$$

Then, the upper limit of the free energy per cluster is given by

$$\begin{aligned} \phi^\nu = & -\frac{1}{\beta} \ln(\text{Tr} e^{-\beta H_0^\nu}) - \frac{J_A}{2} \sum_{(i,j')} \langle S_i \rangle_0 \langle S_{j'} \rangle_0 \\ & - J_B \sum_{\langle(i,j',k) \rangle} \langle (1 - S_i^2) S_k \rangle_0 \langle S_{j'} \rangle_0 \\ & + \sum_{i \in \nu} \eta_i \langle S_i \rangle_0 + \sum_{(i,k \in \nu)} \lambda_{i,k} \langle S_i^2 S_k \rangle_0, \end{aligned} \quad (8)$$

where  $\beta = 1/T$ . In the following, we discuss the CMF solution for each long-range order observed in the model.

In the antiferromagnetic solution, the clusters are identical due to the periodicity two of the phase. It means that the site  $i$  in a cluster  $\nu$  is equivalent to the site  $i'$  in the cluster  $\nu'$ , i.e.,  $\langle S_i \rangle_0 = \langle S_{i'} \rangle_0$ . For the SAF phase, however, equivalent sites from neighbor clusters show local magnetizations of opposite signs, as shown in Fig. 1(a). Therefore, we considered that  $\langle S_i \rangle_0 = -\langle S_{i'} \rangle_0$  for the SAF solution. Then, minimization of Eq. (8) leads to the effective Hamiltonian of the AF/SAF phase

$$\begin{aligned} H_{\text{eff}}^{\text{AF/SAF}} = & H_{\text{in}} \mp J_A \sum_{(i,j \in \nu)} S_i m_j \\ & \mp J_B \sum_{(i,j \in \nu)} S_i [(2 - S_j^2) m_i - C_{ji}], \end{aligned} \quad (9)$$

where the upper (lower) signs account for the AF (SAF) solution. In addition,

$$m_i = \langle S_i \rangle = \frac{\text{Tr} S_i e^{-\beta H_{\text{eff}}^{\text{AF/SAF}}}}{\text{Tr} e^{-\beta H_{\text{eff}}^{\text{AF/SAF}}}} \quad (10)$$

and

$$C_{ji} = \langle S_j^2 S_i \rangle = \frac{\text{Tr} S_j^2 S_i e^{-\beta H_{\text{eff}}^{\text{AF/SAF}}}}{\text{Tr} e^{-\beta H_{\text{eff}}^{\text{AF/SAF}}}}. \quad (11)$$

After solving the self-consistent Eqs. (9), (10), and (11), one can compute the free-energy of the AF/SAF solution, which is given by

$$\begin{aligned} \phi_{\text{AF/SAF}}^\nu = & -\frac{1}{\beta} \ln(\text{Tr} e^{-\beta H_{\text{eff}}^{\text{AF/SAF}}}) \pm J_A \sum_{(i,j \in \nu)} m_i m_j \\ & \pm J_B \sum_{(i,j \in \nu)} m_i (m_i - C_{ji}). \end{aligned} \quad (12)$$

It is important to point out that the orders can also be identified by considering sums and differences of local magnetizations [30]. In particular, the thermodynamic phases can be described by the following order parameters:  $m_A = (m_1 + m_2 + m_3 + m_4)/4$  and  $m_B = (|m_1 - m_2| + |m_3 - m_4|)/4$ . For instance, the AF phase occurs when  $m_A = 0$  and  $m_B \neq 0$ . The SAF order is characterized by  $m_A \neq 0$  and  $m_B \neq 0$ , while the PM phase presents  $m_A = 0$  and  $m_B = 0$ .

As will be discussed in the following section, we also find a cluster antiferromagnetic state, in which the local magnetizations follow the pattern depicted in Fig. 4, with order parameters  $m_A \neq 0$  and  $m_B = 0$ . For the cluster of size  $n_s = 4$ , the relation  $\langle S_i \rangle_0 = -\langle S_{i'} \rangle_0$  is also valid, which means the cluster antiferromagnetic solution could be obtained by using the equations of the SAF solution.

### III. RESULTS AND DISCUSSION

We computed the different self-consistent solutions for the mean-field parameters and, then, used the local magnetizations and the free-energy to locate the phase boundaries. This allowed us to evaluate phase diagrams of the temperature versus the crystal field at three levels of approximation, namely, for cluster sizes  $n_s = 1, 4$ , and  $8$ . We start by analyzing the case where the cluster has size  $n_s = 1$ , i.e., within the usual mean-field approach. It is important to remark that in this case, as each cluster has a single site, we solved the self-consistent mean-field equations for four clusters to capture the AF and SAF symmetries.

Figure 2 exhibits the phase diagram within the single-site mean-field level. We note that AF and SAF phases can be found at low temperatures, depending on the crystal field value. At zero temperature, the system is found in the AF state for  $D/|J_A| \geq 0$  and in the SAF state for  $-4 \leq D/|J_A| \leq 0$ . For  $D/|J_A| \leq -4$ , a zero-temperature PM state is observed, as a consequence of the nonmagnetic states favored by the crystal field. It is worth to mention that the ground-state description is in agreement with the Monte Carlo results and the MF calculations from Ref. [10]. We also note that thermal fluctuations can lead to the onset of a PM state. In particular, the SAF phase is found in a domelike structure in the phase diagram, as suggested by the Monte Carlo results. Moreover,

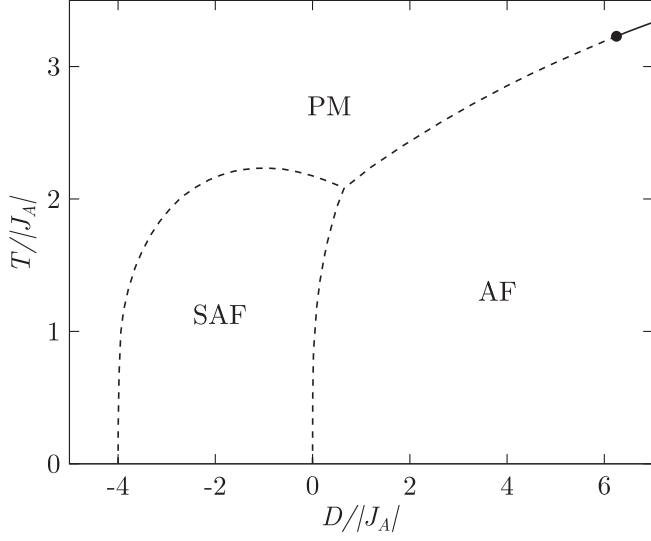


FIG. 2. Phase diagram of  $T/|J_A|$  vs  $D/|J_A|$  for  $n_s = 1$ . Dashed and solid lines represent first-order and second-order phase transitions, respectively. The circle represents the tricritical point.

the MF findings indicate that the transitions between the SAF phase and other phases are discontinuous. However, the phase boundary between paramagnetic and antiferromagnetic phases exhibit both continuous and discontinuous phase transitions, with a tricritical point near  $(D/|J_A|, T/|J_A|) = (6.25, 3.23)$ . We note that this tricritical point is found at larger values of crystal field when compared to the findings of Ref. [10]. This divergence in the results occurs because in the present work we allowed thermally dependent local densities in the AF solution. It is also important to remark that in the Ising limit, i.e., when  $D \rightarrow \infty$ , our analysis gives a finite Néel temperature ( $T_N/|J_A| = 4$ ), which is in agreement with previous mean-field results [31]. We note that the nature of phase transitions at the mean-field level are rather different from the Monte Carlo findings [10]. In particular, the simulations in Ref. [10] indicate that only second-order phase transitions occur between PM and AF phases and that the PM-SAF phase boundary exhibits both first- and second-order phase transitions. This suggests that it is necessary to go beyond the single-site mean-field treatment to improve the description of the present model.

As an attempt to improve the canonical mean-field treatment, we first consider a cluster mean-field approach with  $n_s = 4$ . In this case, the phase diagram (see Fig. 3) exhibits several differences when compared to the results for  $n_s = 1$ . For instance, second-order AF-PM phase transitions are found for lower values of  $D/|J_A|$ . In particular, tricriticality occurs for  $D/|J_A| \approx 0.9$ .

Surprisingly, we also found a magnetic order not previously reported for this model. This magnetic state, here referred as cluster antiferromagnetic (CAF) phase, is found between the SAF phase and the high-temperature paramagnetic state. In the CAF phase, the local magnetizations exhibit a pattern with the formation of four-site square plaquettes, as shown in Fig. 4.

To better describe the CAF phase, we investigate some relevant properties of this order, such as the local magneti-

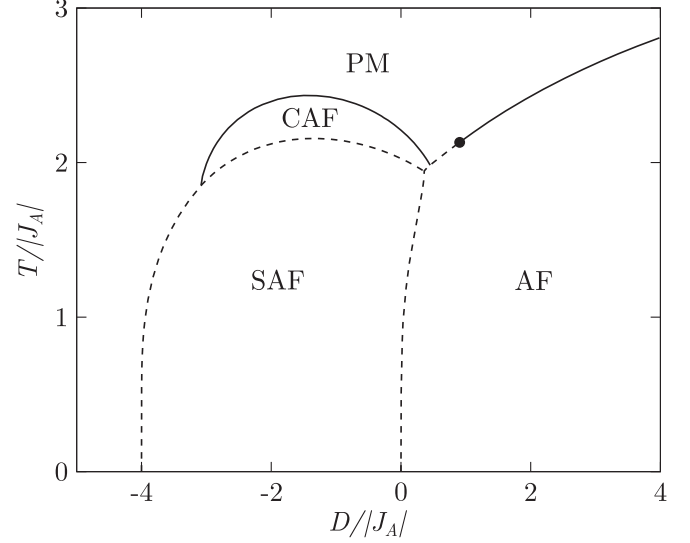


FIG. 3. Phase diagram of  $T/|J_A|$  vs  $D/|J_A|$  for  $n_s = 4$ . Dashed and solid lines represent, respectively, first and second-order phase transitions. The tricritical point is indicated by the filled circle.

zations and the correlations  $C_{ij}$ . Figure 5(a) shows the local magnetizations for  $D/|J_A| = -2$ , where a first-order phase transition between SAF and CAF phases is driven by thermal fluctuations. We note that in the ground-state, the sites 2 and 3 present zero magnetization. However, thermal fluctuations lead to a finite magnetization on these sites even within the SAF phase. In particular, near the SAF-CAF phase transition, all the local magnetizations show a strong dependence on temperature. In the CAF phase, the local magnetizations show a finite value, which decreases with the increase of temperature until it vanishes at a second-order phase transition to a PM phase. The analysis of the local magnetizations, may suggest the correlations  $C_{ij}$  in the CAF phase should exhibit a larger value when compared to the SAF phase. However, our findings show that the correlation  $\langle S_2^z S_1^z \rangle$  is significantly reduced as the system enters in the CAF phase [see Fig. 5(b)]. Overall, the CAF phase shows very low values for the correlations  $C_{ij}$ .

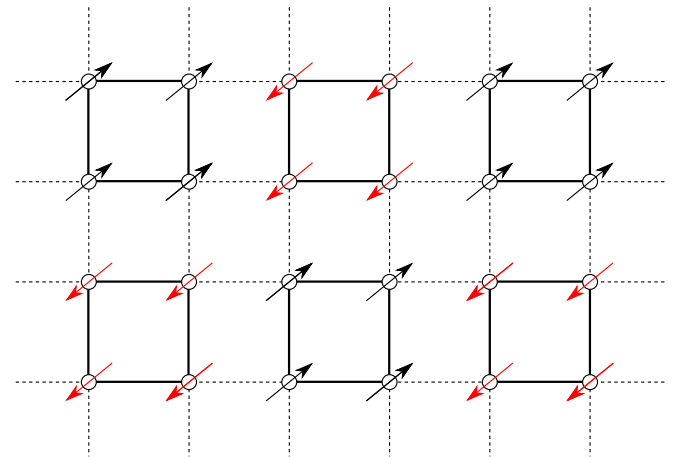


FIG. 4. Representation of the cluster antiferromagnetic order for  $n_s = 4$ .

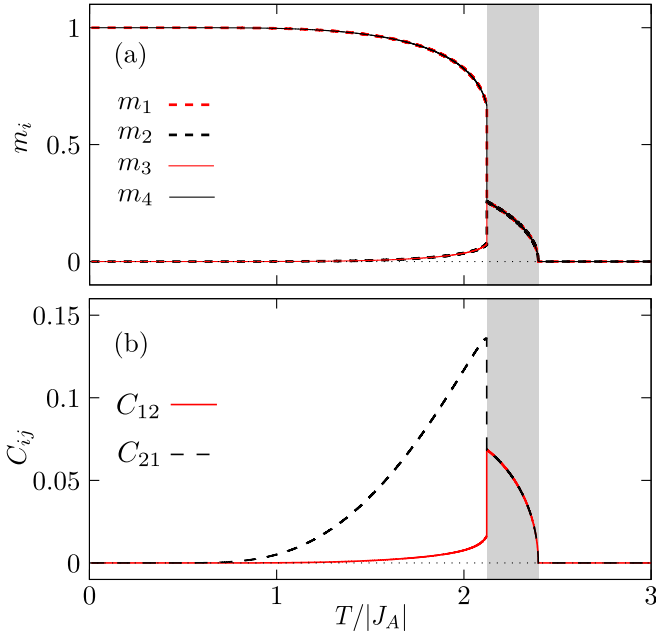


FIG. 5. Thermal dependence of (a) local magnetizations and (b) correlations for  $D/|J_A| = -2$  and  $n_s = 4$ . The gray region indicates the range of temperature in which the CAF phase is stable.

Therefore, a more complete description of this phase requires an analysis of the spin states that are relevant for this type of ordering.

In this way, we investigate the probability of spin states as a function of temperature for  $D/|J_A| = -2$  (see Fig. 6). For a cluster state  $\sigma$  described by spins  $(S_1, S_2, S_3, S_4)$  [see Fig. 1(a)], the probability of this state is given by  $P_\sigma = e^{-\beta E_\sigma} / Z$ , where  $E_\sigma$  is the energy related to this state and  $Z$  is

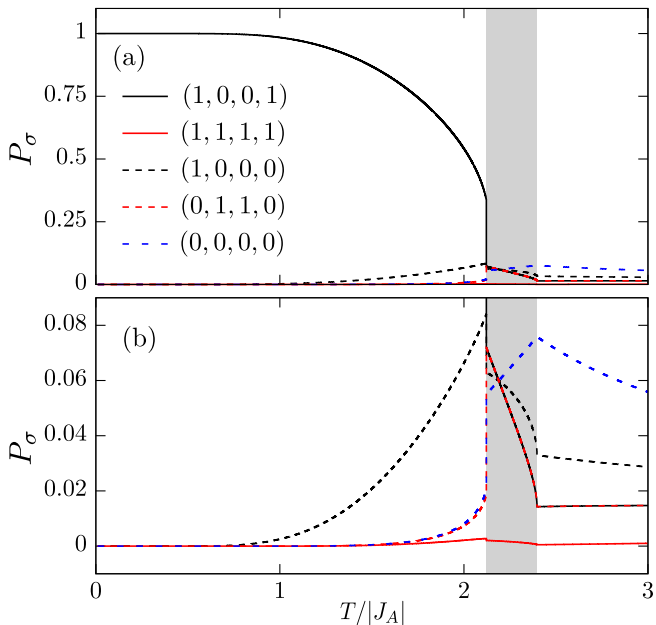


FIG. 6. Probability of different spin states as a function of temperature for  $D/|J_A| = -2$  and  $n_s = 4$ . The gray region indicates the range of temperature in which the CAF phase is stable.

the partition function. We found that as  $T \rightarrow 0$  the probability  $P_{(1,0,0,1)} \rightarrow 1$ , in agreement with the behavior of the local magnetizations [see Fig. 6(a)]. Moreover, the probability of other states is also increased by temperature, which is an expected outcome of thermal fluctuations.

In the CAF region, based on the local magnetizations, one could expect that the probability of the state  $\sigma = (1, 1, 1, 1)$  should be greater than the probability of other states. However, we found that this state has low probability, being very close to zero [see Fig. 6(b)]. The high probability of these states can be clarified by considering the competitive scenario and the role of thermal fluctuations. In particular, the crystal field favors only nonmagnetic sites while  $J_B$  favors states in which half the sites are magnetic. Therefore, the state  $\sigma = (1, 1, 1, 1)$  is not favored neither by  $D$  nor by  $J_B$ , making it very unlikely. In this context, thermal fluctuations yield a highly degenerate phase in which nonmagnetic and magnetic sites play a significant role. For example, the states with only one magnetic site [ $\sigma = (1, 0, 0, 0)$ ,  $(0, 1, 0, 0)$ ,  $(0, 0, 1, 0)$  and  $(0, 0, 0, 1)$ ] are of large probability. These results explain the low values for the correlations and local magnetizations within the CAF thermodynamic phase, as shown in Fig. 5. Thereby, we propose that the CAF phase is a thermally driven degenerate state. We also note that the probability of relevant states with magnetic sites is reduced as temperature is increased and the CAF-PM phase transition is approached. However, the probability of  $\sigma = (0, 0, 0, 0)$  shows a maximum at the phase transition, indicating that nonmagnetic states play a significant role near the CAF-PM phase transition.

A relevant quantity in the description of the present model is the density of magnetic sites, which is given by

$$\rho = \frac{1}{n_s} \sum_{i \in v} \rho_i, \quad (13)$$

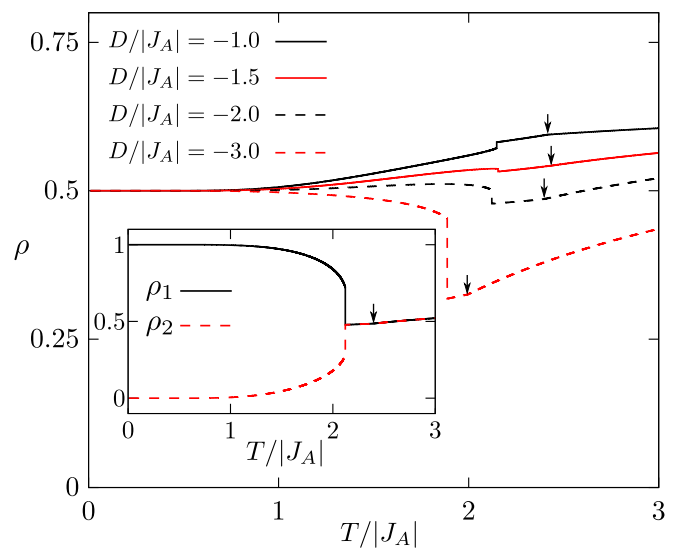


FIG. 7. Thermal dependence of the density of magnetic sites for several values of  $D/|J_A|$ . Inset: local density of magnetic sites as a function of temperature for  $n_s = 4$  and  $D/|J_A| = -2$ . An arrow indicates the temperature of the transition between CAF and PM phases.

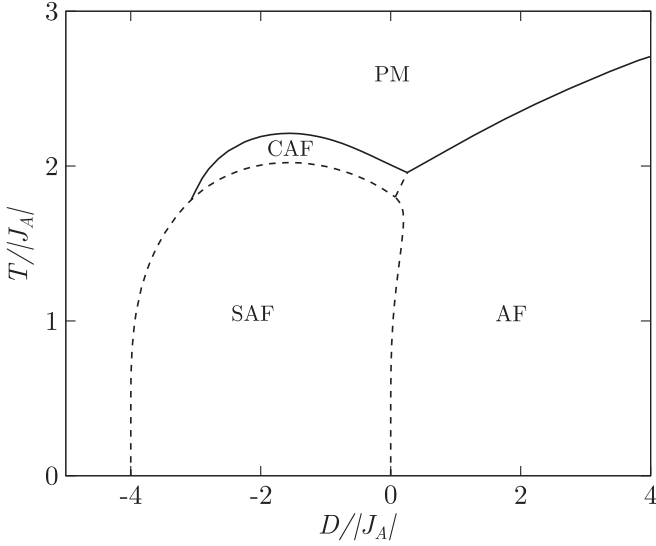


FIG. 8. Phase diagram of  $T/|J_A|$  vs  $D/|J_A|$  for  $n_s = 8$ . Dashed and solid lines represent, respectively, first- and second-order phase transitions.

where  $\rho_i = \langle S_i^2 \rangle$  are local densities. In Fig. 7, we present  $\rho$  as a function of temperature for different values of  $D/|J_A|$  and  $n_s = 4$ . We observe a discontinuity in  $\rho$  at the SAF-CAF transition, which occurs due to the first-order nature of this phase transition. However, a much more subtle change in density is observed at the CAF-PM transition. This could be attributed to the second-order nature of the phase transition and that in both phases a variety of spin states are relevant. It is worth to remark that our findings for  $\rho$  are in good agreement with the Monte Carlo simulation [10] for this model. Despite the CAF phase is not reported in Ref. [10], we note that the density is not the ideal parameter to identify a CAF-PM transition, specially when error bars should be taken into account, as in Monte Carlo methods. In the inset of Fig. 7, we show

the thermal dependence of the local density of magnetic sites ( $\langle S_i^2 \rangle$ ) for the sites one and two. We note that in the SAF phase, the local densities are different on sites belonging to different sublattices, contrary to what occurs in the CAF phase, in which all the local densities are identical. It means that the difference between local densities of nearest-neighbors could be a useful tool to identify whether the system is on a SAF or CAF state.

To prevent a possible effect of the particular choice of cluster on the CMF outcomes, we investigate clusters of sizes  $n_s = 8$  [see Fig. 1(b)] and  $n_s = 12$  (see Fig. 11). The phase diagram obtained within the  $n_s = 8$  approximation is shown in Fig. 8. As a result, we find that the PM-AF phase boundary shows only second-order phase transitions, which is in qualitative agreement with the Monte Carlo simulations [10]. Moreover, the CAF phase is still found at intermediate temperatures, which indicates that this state is not an artifact of the cluster size adopted within the CMF theory. However, we remark that the CAF region is moderately reduced when compared with the  $n_s = 4$  approximation. Since the mean-field-like methods usually overestimate the ordering temperatures, a small reduction in the CAF region, as the approximation is improved, is expected. However, it also raises a question on whether the presence of the CAF phase is robust under the increase of  $n_s$ .

To shed some light on this question, we investigate the local magnetizations behavior in a  $n_s = 12$  cluster for different values of  $D/|J_A|$ . In Fig. 9, we show a comparative between the magnetizations of topologically equivalent sites for  $n_s = 12$  (see Fig. 11) and  $n_s = 8$ , as well as the order parameters for  $n_s = 4$ . We note that the CAF region is slightly reduced when the cluster increases from  $n_s = 8$  to  $n_s = 12$ , indicating that the CAF phase remains present for larger  $n_s$ . Also, we observe a more noticeable decrease in the CAF region for lower values of  $D$ , indicating that the CAF region might be slightly displaced toward larger values of  $D/|J_A|$ .

We also note that the nature of the phase transitions involving SAF, CAF and PM phases are the same for  $n_s = 4$ ,

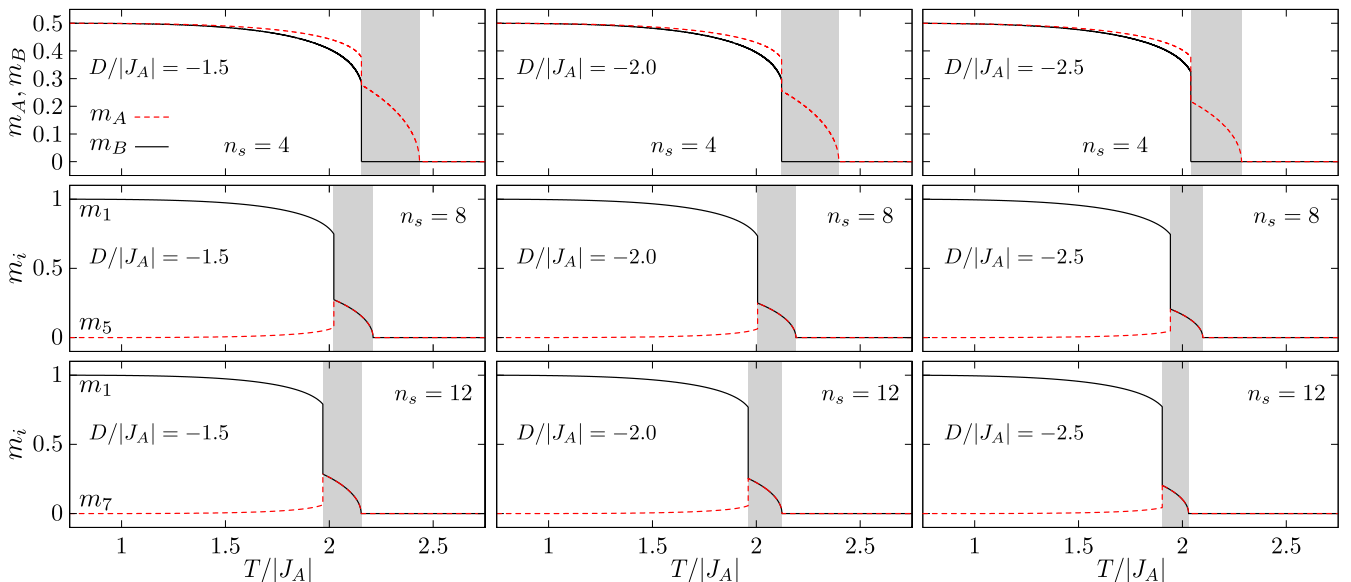


FIG. 9. Thermal dependence of order parameters for  $n_s = 4$  and local magnetizations for  $n_s = 8$  and 12 (see Fig. 11) at different values of  $D/|J_A|$ :  $-1.5$ ,  $-2.0$ , and  $-2.5$ . The gray regions indicate the temperature ranges of the CAF phase.

8, and 12. In particular, the ground-state description remains unchanged within all the different levels of approximation adopted.

#### IV. CONCLUSIONS

We investigate a three-state spin model with competing interactions, including a hole-mediated coupling, proposed recently in Ref. [10]. Our central goal was to describe the temperature versus crystal field phase diagram of the model, which is expected to reproduce some features from the phase diagrams of high- $T_c$  superconductors [12,32]. To provide a picture beyond the standard mean-field theory, we employ a cluster mean-field method that allows us to incorporate short-range correlations in the model description.

Our CMF results indicate that the PM-AF phase boundary shows only second-order phase transitions, which agree with the Monte Carlo findings and differs from the single-site mean-field description [10]. Moreover, our calculations indicate only first-order phase transitions between AF and SAF orders. We remark that the Monte Carlo description of these phase boundaries is rather tricky [10], which means our findings provide an important benchmark for the model.

In addition, we found a thermally driven ordered state, named CAF state, which is not reported in previous investigations of the model [10]. Our findings suggest that the CAF phase is characterized by low values of local magnetizations and correlations. Moreover, this phase can be described as a degenerate state, in which several spin states have a high probability of occurrence. In fact, these features suggest that describing this phase within Monte Carlo simulations could be very intricate. For instance, the finite-size effects on simulations can prevent the use of small local magnetizations to identify long-range orders, as the CAF phase. In addition, we find that the transition between CAF and other ordered states are of first-order, while the CAF-PM transitions are always of second-order.

In our opinion, the rich phenomenology arising from this model is a topic worth of further investigations. Despite we consider different cluster sizes in our approach, other approximations, such as effective-field theory [33], cluster variation method [34] and correlated cluster mean-field theory [31], could be adopted to investigate our findings. For instance, the onset and stability of the CAF phase are particularly relevant subjects, and could be analyzed by other methods [35].

Furthermore, extensions of the present model can unveil other interesting properties. For instance, the inclusion of second-neighbor antiferromagnetic couplings can lead to other relevant phenomena, as suggested by Ref. [10]. We note that the CMF method was recently applied to the  $J_1$ - $J_2$  Ising model on the square lattice for both spin-1/2 [18] and spin-1 [36]. Moreover, the CMF description of the thermally driven phase transitions on the spin-1/2 version of this model shows good agreement with recent Monte Carlo findings [18]. This suggests the CMF method is suitable to investigate the role of second-neighbor couplings on the CS model.

#### ACKNOWLEDGMENT

This work was supported by the Brazilian agencies Conselho Nacional de Desenvolvimento Científico e Tecnológico

(CNPq) and Fundação de Amparo à Pesquisa do Estado do Rio Grande do Sul (Fapergs).

#### APPENDIX A: $n_s = 1$

In the usual mean-field treatment the reference system is a set of noninteracting sites on a square lattice. To describe the AF and SAF phases, we solved the mean-field equations for four different sites, as represented in Fig. 10. In this way, the four-site Hamiltonian is given by

$$H_0^v = - \sum_{i \in v} (\eta_i S_i + \lambda_i S_i^2 + D S_i^2). \quad (\text{A1})$$

The original system follows Eq. (5), where the averages can be expressed as

$$\langle S_i S_{j'} \rangle_0 = \langle S_i \rangle_0 \langle S_{j'} \rangle_0, \quad (\text{A2})$$

and

$$\langle (1 - S_i^2) S_k S_{j'} \rangle_0 = \langle (1 - S_i^2) \rangle_0 \langle S_k \rangle_0 \langle S_{j'} \rangle_0. \quad (\text{A3})$$

We note that the labels introduced in Fig. 10 allows to relate the local properties from cluster  $v$  and its neighbors (such as  $v'$ ). In particular, for the AF solution we have  $\langle S_i \rangle_0 = \langle S_{i'} \rangle_0$  and the minimization of the free-energy upper bound leads to the effective Hamiltonian

$$H_{\text{eff}}^{\text{AF}} = - 2J_A \sum_{(i,j \in v)} S_i m_j - D \sum_{i \in v} S_i^2 - J_B \sum_{(i,j \in v)} S_i [2(1 - \rho_j) m_i - S_i m_j^2], \quad (\text{A4})$$

where  $m_i$  and  $\rho_i$  are local magnetizations and local densities from  $v$ . The four-site free energy is given by

$$\phi_{AF}^v = - \frac{1}{\beta} \ln (\text{Tr} e^{-\beta H_{\text{eff}}^{\text{AF}}}) + J_A \sum_{(i,j \in v)} m_i m_j + 2J_B \sum_{(i,j \in v)} m_i^2 \left( \frac{1}{2} - \rho_j \right). \quad (\text{A5})$$

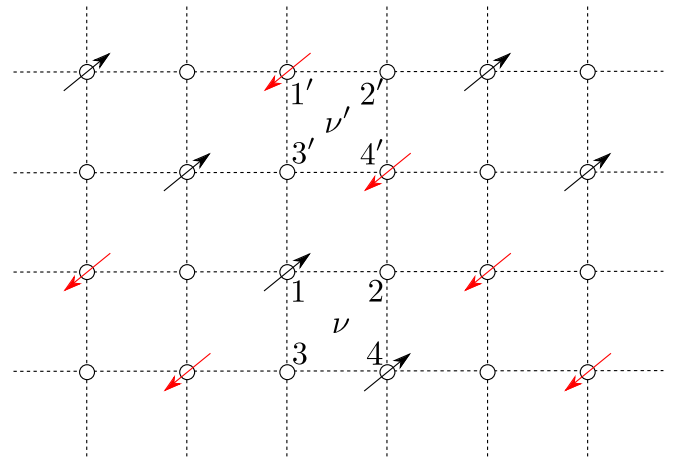


FIG. 10. Representation of the clusters considered in the CMF approach with  $n_s = 1$ .

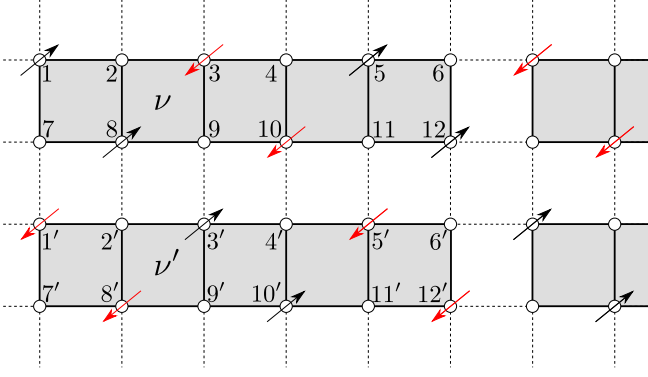


FIG. 11. Representation of the clusters considered in the CMF approach with  $n_s = 12$ .

For the SAF solution we consider  $\langle S_i \rangle_0 = -\langle S_{i'} \rangle_0$ , which results in the effective Hamiltonian given by

$$H_{\text{eff}}^{\text{SAF}} = J_B \sum_{(i,j \in \nu)} S_i [2(1 - \rho_j) m_i - S_i m_j^2] - D \sum_{i \in \nu} S_i^2. \quad (\text{A6})$$

The four-site free-energy of the SAF solution is given by

$$\phi_{\text{SAF}}^{\nu} = -\frac{1}{\beta} \ln (\text{Tre}^{-\beta H_{\text{eff}}^{\text{SAF}}}) - 2J_B \sum_{(i,j \in \nu)} m_i^2 \left( \frac{1}{2} - \rho_j \right). \quad (\text{A7})$$

#### APPENDIX B: $n_s = 8$

For  $n_s = 8$ , our reference system is a square lattice divided in identical clusters as illustrated in Fig. 1(b). This cluster allows to incorporate exactly some couplings between third neighbors, which allows us to improve over the four-site approximation. The Hamiltonian of a single cluster  $\nu$  is then

given by Eq. (3) with

$$H_{\text{in}} = -J_A \sum_{(i,j \in \nu)} S_i S_j - J_B \sum_{\langle\langle i,j,k \in \nu \rangle\rangle} (1 - S_i^2) S_j S_k - D \sum_{i \in \nu} S_i^2. \quad (\text{B1})$$

It should be noted that each cluster is connected to four nearest-neighbor clusters, as in the  $n_s = 1$  and  $n_s = 4$  cases. Here, however, we have two types of clusters  $\nu$  and  $\nu'$  in the neighborhood of  $\nu$ , as shown in Fig. 1(b). This distinction is necessary due to the magnetization pattern in the SAF and CAF phases.

The average of the Hamiltonian of the original system is given by

$$\langle H^{\nu} \rangle_0 = \langle H_{\text{in}} \rangle_0 - \frac{J_A}{2} \sum_{(i,j')} \langle S_i S_{j'} \rangle_0 - J_B \sum_{\langle\langle i,j',k \rangle\rangle} \langle (1 - S_i^2) S_{j'} S_k \rangle_0, \quad (\text{B2})$$

where the averages can be expressed as in Eqs. (6) and (7). In the AF phase, the local magnetization pattern is identical on each cluster. In other words, for the AF solution we can adopt  $\langle S_i \rangle_0 = \langle S_{i'} \rangle_0 = \langle S_{i''} \rangle_0$ . For the SAF and CAF phases, the clusters connected by horizontal links showed the same pattern of local magnetizations, while the clusters connected by vertical links showed local magnetizations of opposite sign on equivalent sites. Therefore, we considered  $\langle S_i \rangle_0 = \langle S_{i''} \rangle_0$  and  $\langle S_{i'} \rangle_0 = -\langle S_i \rangle_0$ . Minimization of Eq. (2) with respect to the variational parameters allows us to write the effective Hamiltonian and free-energy for the AF/SAF phases as

$$H_{\text{eff}}^{\text{AF/SAF}} = H_{\text{in}} - J_A [S_1(m_4 \pm m_5) \pm S_2 m_6 \pm S_3 m_7 + S_4(m_1 \pm m_8) + S_5(m_8 \pm m_1) \pm S_6 m_2 \pm S_7 m_3 + S_8(m_5 \pm m_4)] \pm J_B [S_1^2(S_5 m_5 \pm S_2 m_4) + S_2^2 S_6 m_6 + S_3^2 S_7 m_7 + S_4^2(S_8 m_8 \pm S_3 m_1) + S_5^2(S_1 m_1 \pm S_6 m_8) + S_6^2 S_2 m_2 + S_7^2 S_3 m_3 + S_8^2(S_4 m_4 \pm S_7 m_5)] - J_B [S_1(m_3 \pm 2m_1 - C_{4,3} \mp C_{5,1}) + S_2(m_4 \pm 2m_2 \mp C_{6,2}) + S_3(m_1 \pm 2m_3 \mp C_{7,3}) + S_4(m_2 \pm 2m_4 - C_{1,2} \mp C_{8,4}) + S_5(m_7 \pm 2m_5 - C_{8,7} \mp C_{1,5}) + S_6(m_8 \pm 2m_6 \mp C_{2,6}) + S_7(m_5 \pm 2m_7 \mp C_{3,7}) + S_8(m_6 \pm 2m_8 - C_{5,6} \mp C_{4,8})], \quad (\text{B3})$$

and

$$\phi_{\text{AF/SAF}}^{\nu} = -\frac{1}{\beta} \ln (\text{Tre}^{-\beta H_{\text{eff}}^{\text{AF/SAF}}}) + J_A [m_1(m_4 \pm m_5) + m_8(m_5 \pm m_4) \pm m_2 m_6 \pm m_3 m_7] + J_B [m_1(m_3 \pm m_1 - C_{4,3} \mp C_{5,1}) + m_2(m_4 \pm m_2 \mp C_{6,2}) \pm m_3(m_3 - C_{7,3}) + m_4(\pm m_4 - C_{1,2} \mp C_{8,4}) + m_5(\pm m_5 \mp C_{1,5} - C_{8,7}) \pm m_6(m_6 - C_{2,6}) + m_7(m_5 \pm m_7 \mp C_{3,7}) + m_8(m_6 \pm m_8 - C_{5,6} \mp C_{4,8})], \quad (\text{B4})$$

respectively. It is worth to note that the topological inequivalence of sites for the cluster with  $n_s = 8$  leads to artificial inhomogeneities on the local quantities. As a consequence, an analysis of local densities and magnetizations can be done in

a more straightforward way when the cluster with  $n_s = 4$  is considered, due to the topological equivalence of all the sites in this cluster. For  $n_s = 8$ , one can differ the CAF state from the SAF phase by comparing the local magnetizations. For

instance, the CAF state is described by  $m_1 = m_5 = -m_4 = -m_8$  while the SAF phase shows  $m_1 = -m_8$ ,  $m_5 = -m_4$  and  $m_1 \neq m_5$ .

### APPENDIX C: $n_s = 12$

The CMF approach for the 12-site cluster is a straightforward extension of the method for smaller clusters. The

Hamiltonian of a single cluster  $\nu$  (see Fig. 11) follows Eq. (B1), and its average is given by Eq. (B2). Nevertheless, the AF and SAF solutions follow the same symmetry of the  $n_s = 4$  approximation. It means that, for the AF solution we consider  $\langle S_i \rangle_0 = \langle S_{i'} \rangle_0$ , and for the SAF solution we consider  $\langle S_i \rangle_0 = -\langle S_{i'} \rangle_0$ . Because the final equations for the effective Hamiltonian and free energy are lengthy, their explicit form is omitted.

- 
- [1] A. G. Green, G. Conduit, and F. Krüger, *Annu. Rev. Condens. Matter Phys.* **9**, 59 (2018).
- [2] T. Yamaguchi, S.-L. Drechsler, Y. Ohta, and S. Nishimoto, *Phys. Rev. B* **101**, 104407 (2020).
- [3] M. Gohlke, L. E. Chern, H.-Y. Kee, and Y. B. Kim, *Phys. Rev. Res.* **2**, 043023 (2020).
- [4] N. Schupper and N. M. Shnerb, *Phys. Rev. Lett.* **93**, 037202 (2004).
- [5] O. Portmann, A. Vaterlaus, and D. Pescia, *Nature* **422**, 701 (2003).
- [6] Y. Nahas, S. Prokhorenko, J. Fischer, B. Xu, C. Carretero, S. Prosandeev, M. Bibes, S. Fusil, B. Dkhil, V. Garcia *et al.*, *Nature* **577**, 47 (2020).
- [7] S. Sachdev, *Science* **288**, 475 (2000).
- [8] S. Kirchner, S. Paschen, Q. Chen, S. Wirth, D. Feng, J. D. Thompson, and Q. Si, *Rev. Mod. Phys.* **92**, 011002 (2020).
- [9] I. M. Hayes, N. Maksimovic, G. N. Lopez, M. K. Chan, B. Ramshaw, R. D. McDonald, and J. G. Analytis, *Nat. Phys.* **17**, 58 (2020).
- [10] S. A. Cannas and D. A. Stariolo, *Phys. Rev. E* **99**, 042137 (2019).
- [11] C. Pfeleiderer, *Rev. Mod. Phys.* **81**, 1551 (2009).
- [12] D. J. Scalapino, *Rev. Mod. Phys.* **84**, 1383 (2012).
- [13] L. P. Kadanoff, *J. Stat. Phys.* **137**, 777 (2009).
- [14] S. Jin, A. Sen, and A. W. Sandvik, *Phys. Rev. Lett.* **108**, 045702 (2012).
- [15] A. Kalz and A. Honecker, *Phys. Rev. B* **86**, 134410 (2012).
- [16] A. Singhanian and S. Kumar, *Phys. Rev. B* **101**, 064403 (2020).
- [17] A. Singhanian and S. Kumar, *Phys. Rev. B* **98**, 104429 (2018).
- [18] S. Jin, A. Sen, W. Guo, and A. W. Sandvik, *Phys. Rev. B* **87**, 144406 (2013).
- [19] B. K. Alavani, A. Das, and R. V. Pai, *J. Phys. B: At., Mol. Opt. Phys.* **51**, 145302 (2018).
- [20] B. Javanparast, A. G. R. Day, Z. Hao, and M. J. P. Gingras, *Phys. Rev. B* **91**, 174424 (2015).
- [21] M. Schmidt, F. M. Zimmer, and S. G. Magalhaes, *Phys. Scr.* **90**, 025809 (2015).
- [22] M. Schmidt, N. Kellermann, and F. M. Zimmer, *Phys. Rev. E* **102**, 032139 (2020).
- [23] N. Kellermann, M. Schmidt, and F. M. Zimmer, *Phys. Rev. E* **99**, 012134 (2019).
- [24] D. Yamamoto, H. Ueda, I. Danshita, G. Marmorini, T. Momoi, and T. Shimokawa, *Phys. Rev. B* **96**, 014431 (2017).
- [25] D. Yamamoto, C. Suzuki, G. Marmorini, S. Okazaki, and N. Furukawa, *Phys. Rev. Lett.* **125**, 057204 (2020).
- [26] D. Yamamoto, G. Marmorini, M. Tabata, K. Sakakura, and I. Danshita, *Phys. Rev. B* **100**, 140410(R) (2019).
- [27] Y.-Z. Ren, N.-H. Tong, and X.-C. Xie, *J. Phys.: Condens. Matter* **26**, 115601 (2014).
- [28] D. Yamamoto, G. Marmorini, and I. Danshita, *Phys. Rev. Lett.* **112**, 127203 (2014).
- [29] D. Yamamoto, G. Marmorini, and I. Danshita, *Phys. Rev. Lett.* **114**, 027201 (2015).
- [30] A. I. Guerrero, D. A. Stariolo, and N. G. Almarza, *Phys. Rev. E* **91**, 052123 (2015).
- [31] D. Yamamoto, *Phys. Rev. B* **79**, 144427 (2009).
- [32] B. Keimer, S. A. Kivelson, M. R. Norman, S. Uchida, and J. Zaanen, *Nature* **518**, 179 (2015).
- [33] A. Bobák, E. Jurčíšínová, M. Jurčíšín, and M. Žukovič, *Phys. Rev. E* **97**, 022124 (2018).
- [34] A. I. Guerrero and D. A. Stariolo, *Physica A* **466**, 596 (2017).
- [35] J. Jin, A. Biella, O. Viyuela, L. Mazza, J. Keeling, R. Fazio, and D. Rossini, *Phys. Rev. X* **6**, 031011 (2016).
- [36] T. Balcerzak, K. Szałowski, A. Bobák, and M. Žukovič, *Phys. Rev. E* **98**, 022123 (2018).